Chapter 2
The Alternating Gradient Force Magnetometer

As noted in section 1.2.3, the AGFM is a force instrument, comprising of 3 component parts. Firstly, the instrument must be capable of applying a known magnetic field to the sample. Methods of generating fields of various strengths have been well covered in the literature [1, 2]. Secondly, the instrument must have a controllable source of alternating field gradient. This has conventionally been achieved with coils of appropriate geometry, carrying an alternating current, and is described in more detail in section 2.2.1. Finally, the resulting oscillatory force on the sample has to be detected, usually by attaching the sample to a mechanically compliant system and measuring the displacement. Many of the previously reported systems have operated at a mechanical resonance, thereby greatly enhancing the displacement. This is covered in more detail in sections 2.2.2, and 2.2.3.

2.1 Review of AGFM literature

The physical forms of instruments that could be called AGFM's are diverse, as they have been used to study a range of samples under different conditions, and different geometries. A list of the instruments discussed in this section can be found in Table 2.1, along with details of the detection systems used, some design parameters, and the resolutions obtained. The first demonstration of resonant operation of a force magnetometer was by Zijlstra [3] in 1970. He called his instrument a vibrating reed magnetometer; it was only later that AGFM became the preferred name. Zijlstra designed his instrument in order to study the hysteresis curves of microscopic (a few μm across) single domain particles. Using a fine (38 μm x 20 mm) gold wire as a resonant element, a resolution of 10^{-11} J T^{-1} was reported. Zijlstra's experimental set-up was configured so that the alternating gradient field was oriented vertically, in the same direction as the applied DC field. The resonant element was mounted perpendicular to the field (i.e. horizontally). The displacement of the reed was measured visually, with the aid of a calibrated microscope, and a stroboscopic lamp to 'freeze' the motion of the fibre at its maximum deflection. The signal used to drive the stroboscope

lamp was derived from the same source (an audio oscillator) as that used to drive the gradient coils, after passing through a phase shifting network.

Author	Year	Sample Size	Resolution [J T^{-1}]	Detection Method	Probe Material	Probe dimensions	Q factor	Gradient field [T m^{-1}]	Resonant frequency [Hz]
Zijlstra [3]	1970	~10 μm	10^{-11}	Stroboscope	Fine gold wire	38 μm x 20 mm	100	5	~170
Reeves [4]	1972	several grams	2 x 10^{-10}	Piezoelectric record player cartridge	Silica tubing (non resonant)	3.5 mm x 350 mm	10-100	0.1	167 (operated at ~70)
Roos *et al.,* [5]	1980	~10 μm	10^{-13}	Piezoelectric biomorph	Fine gold wire + glass fibre	18 μm x 10 mm, 150 μm x 70 mm	<70, 550 in vacuum	16.7	62, and 20
Schippan *et al.,* [6]	1982	~10 μm	10^{-13}	Piezoelectric biomorph	Hollow quartz fibre	150 μm OD, 100 μm ID x 30 mm	<70	16.7	151, 953 (harmonic)
Flanders [7]	1988	~0.5 mm	10^{-11}	Piezoelectric biomorph	Various	Various, 10 – 25 mm	25 - 250	0.4	10 – 100
Richter *et al.,* [8]	1988	~1 μm	10^{-14}	Piezoelectric biomorph	Compound hollow quartz fibre	100 μm OD, 20 μm ID x 9.8 mm, 780 μm OD, 350 μm ID x 35 mm	310	46.5	852
Frey *et al.,* [9]	1988	100 mm^3	10^{-10}	Piezoelectric biomorph	Double quartz fibre			2.5	40 – 80
Flanders [10]	1990	135 mg	10^{-11}	Piezoelectric biomorph	Quartz fibre (non resonant)	70 – 300 μm x 150 mm	20 - 100	0.4	200 – 550
Gibson *et al.,* [11]	1991	~10 μm	1.4 x 10^{-14}	Optical Interferometry	Magnetic force microscope tip (Si_3N_4)	-	43	50	24500
O'Grady *et al.,* [12]	1993	100 mg	2 x 10^{-11}	Piezoelectric biomorph		-		0.4	500
Wallace *et al.,* [13]	1995	0.5 mm	10^{-8}	Tunnelling current	Brass strip	-	30	0.001	217
Zimmer-mann *et al.,* [14]	1996	~1 μm	10^{-14}	Optical deflection (PSD)	Optic Fibre	125 μm	400	3.2	~1000
Asti *et al.,* [15, 16]	1996	~1 mm	5 x 10^{-10}	Piezoelectric record player cartridge	Tensioned tungsten wire	300 mm x 40 μm	1000	-	150
Hill *et al.,* [17]	1996	Thin films 4 mm x 4 mm	3.4 x 10^{-10}	Optical deflection (PSD)	Tungsten wire	20 mm x 250 μm	700	0.2	250
Ashcroft	2001	various	5 x 10^{-11}	Piezoelectric biomorph	Compound quartz fibre	120 mm x 650 μm	50 - 300	15	40 - 95

Table 2.1. Parameters of previous instruments reported in the literature, and the present work.

Major deveopments in the design of the AGFM were made by Flanders who changed to a different coil configuration [10], employing an alternating field with a gradient perpendicular to the field vector. This is shown in Figure 2.1, and allowed the use of a non-resonant extension, similar to that used earlier by Reeves [4]. This was especially advantageous, as it allowed the resonant element

and piezoelectric biomorph to remain at room temperature, while the temperature of the sample was varied in the range 77 to 900 K. This largely negated the need for a nulling coil (impractical at 900 K), or excessive frequency tracking during experiments, as the resonant properties were found to be nearly stable when using a long extension (100 – 150 mm), that had been suitably heat-shielded. Quartz fibres and capillary tubes were used as extensions, with diameters suited to the sample mass and sensitivity required, in the range 70 μm to 300 μm. The biomorphs used were the only resonant element present, and were of the order of 20 mm long and 0.6 mm thick.

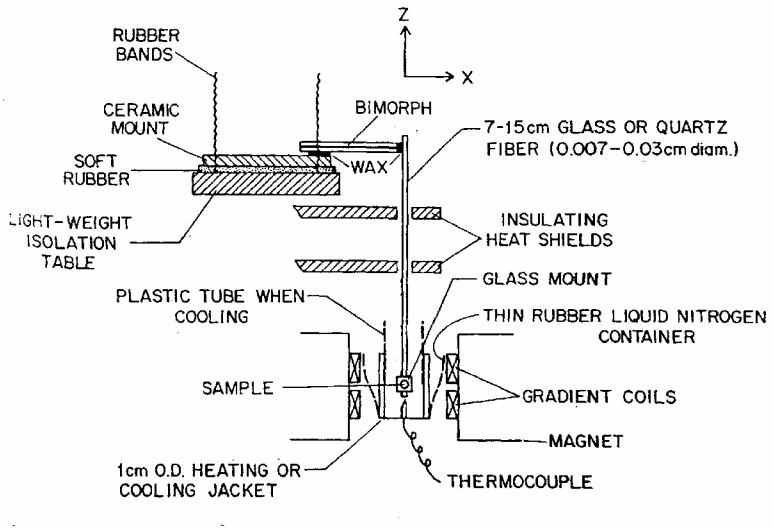

Figure 2.1. The instrument used by Flanders, configured for vertical force mode. (Figure 1 from Flanders [10])

Temperature was varied in a similar manner to that used in previous work [7], with higher temperatures being produced by a furnace of similar size to the cooling tube. Temperatures were measured using a thermocouple mounted just below the sample. The resonant frequency of the system was found to depend strongly on sample mass, decreasing from approximately 500 Hz unloaded, to approximately 200 Hz for a sample of 135 mg, and weakly dependent on temperature when using thin fibres. There was no measurable change in the Q factor with changes in sample temperature. Palladium foil was used to calibrate the system, and to check the resolution obtainable (10^{-11} J T^{-1}). Problems were encountered when measuring superconducting samples, due to unwanted field gradient components in directions perpendicular to the one required. These unwanted components were a necessary consequence of the coil design

employed. This meant that there were very large distortions in measured *M-H* loops when the sample was slightly displaced from the field centre, or for large samples of superconducting material.

In the late 1980's, Princeton Measurements Corp. started producing commercially available AGFM systems, one of which (the M2900 model) was the subject of a paper by O'Grady *et al.,* [12]. In this, a study of the resolution and reproducibility was reported, as well as the effect of the alternating gradient field on samples. This effect was reported to be considerable in the case of samples with a low coercivity, mainly due to sample positioning errors. Deviation of the sample from the centre of the alternating gradient region means that the sample experiences an additional alternating magnetic field component. The commercial system was similar in many respects to Flanders' instruments [7, 10], with a choice of probes corresponding to the two configurations outlined. The resolution was reported as 2×10^{-11} J T^{-1}, slightly worse than the manufacturer's quoted value of 10^{-11} J T^{-1}. Repeatability was within 6 %, deteriorating to 20 % for samples with low moments (towards the limit of resolution). In addition, a low temperature modification was detailed, allowing measurements down to 4 K. This was fabricated from a modified Oxford Instruments ESR continuous flow cryostat. The cooling was performed by a method similar to Flanders [7, 10], whereby a jet of cold gas was directed at the base of an aluminium cup surrounding the sample holder. The flow of helium introduced mechanical noise into the system, reducing the resolution to 2×10^{-8} J T^{-1} at 5 K.

Many authors indulged in calculations of the theoretical resolution of their instruments, limited by such factors as electrical noise in detectors, thermally induced noise in the resonant element, noise base of lock-in amplifiers, etc. In all cases, the actual performance fell considerably short of these predictions. Most authors attributed this to external mechanical vibrations being coupled to the system, despite many taking great care to isolate their systems from the environment. There seems to be at present no way of eliminating this source of noise completely.

2.2 AGFM design

The original motivation for construction of an AGFM has been detailed in section 1.2.1, resulting in a target resolution of 10^{-8} J T^{-1} kg^{-1} or better. It was decided to initially develop the instrument for ambient temperature operation, with a view to subsequently extending operation to cryogenic temperatures. This enabled initial characterisation of the instrument (reported in chapter 3), without the expense of a cryogen supply. Once a room temperature system was established, adaptation to enable measurements down to 77 K was attempted. Cost was also a major influence in many of the design decisions taken, with a limited budget available for development work. The $Hg_{1-x}Mn_xTe$ film samples available were ~0.5 mm thick (including substrate), between 3 and 10 mm across, and were all less than 0.3 grams in weight. The AGFM was therefore designed to accommodate such samples. A conventional iron yoke electromagnet was used, capable of generating homogenous fields up to 400 mT. A schematic of the AGFM is shown in Figure 2.2.

2.2.1 AC magnetic field gradient

The object of the AC gradient coils is to produce a homogenous, well-defined alternating field gradient at an accurately controlled frequency. Field gradient ($\nabla\underline{H}$) is a tensor of rank 2, and has 9 components. One of these components needs to be non zero, as the driving component. It is desirable for the other 8 components to be zero in the region of the sample. Generally this is not possible, so those components that could excite unwanted resonances should be minimised, ideally to a level below that which the instrument is able to detect. A comprehensive study of many coil configurations has been undertaken by Roos *et al.,* [5]. All the previous designs have used circular coils, except Zimmermann *et al.,* [14], where rectangular coils were used. There have been several problems reported [5, 8, 13, 14] of the gradient coils vibrating in a steady applied field, at the driving frequency. The coil winding therefore needed to be held rigid to minimise vibration, as this could disturb a sensitive detector.
A rigid mounting to the pole pieces, and having small coils reduced this problem. A pair of coils were designed, and manufactured in the departmental workshop. The formers were fabricated in Tufnol, with a low magnetic susceptibility, and is

tough, durable, and cheap. It was decided to have a coil of outside diameter 25 mm, inside diameter 6 mm, and thickness 6 mm.

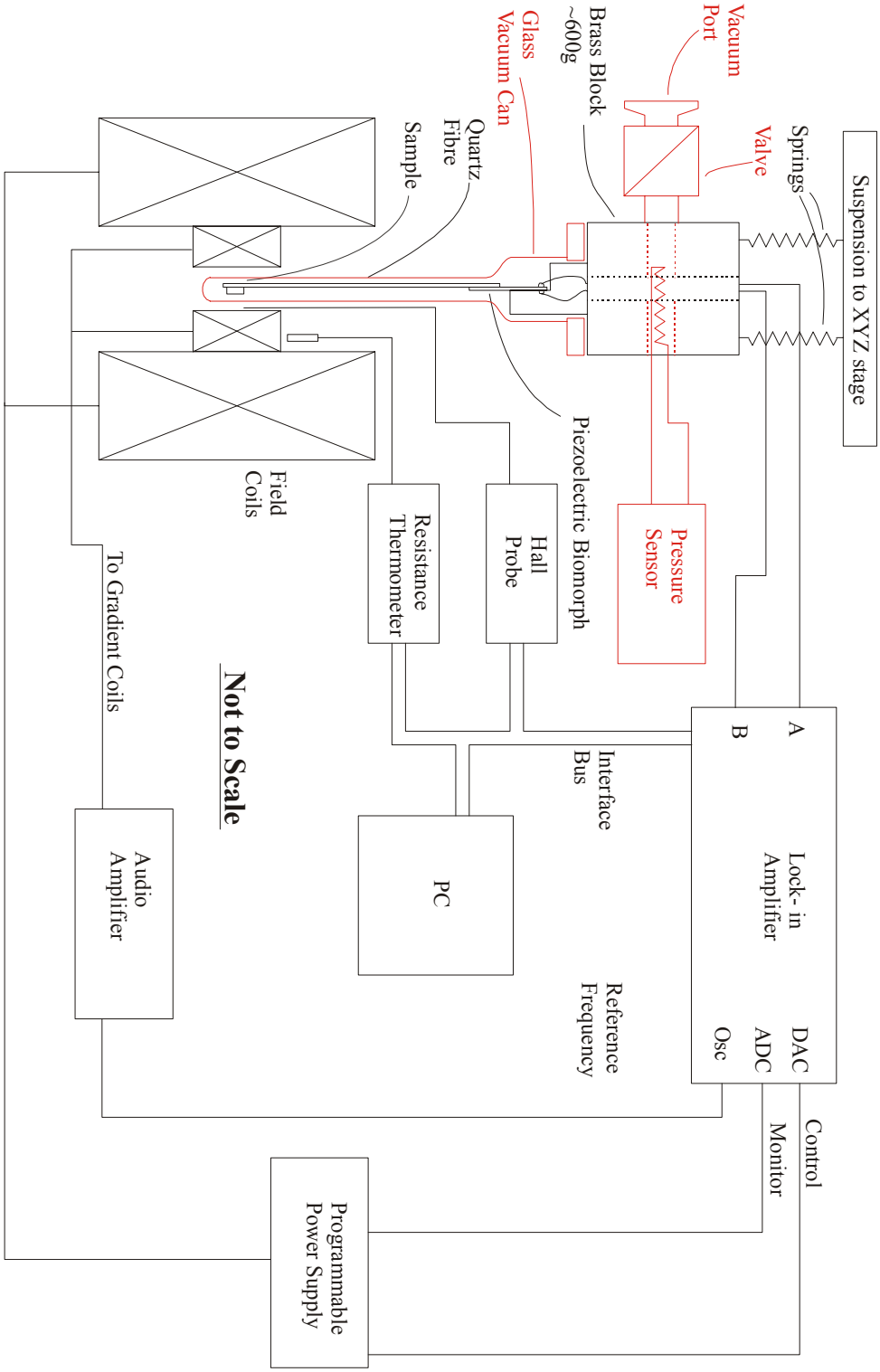

Figure 2.2. Schematic of the AGFM. The new vacuum system is outlined in red.

The coil space had a volume of 2.78 x 10^{-6} m^3, and contained 200 turns of 0.4 mm diameter insulated copper wire, secured with a varnish layer on the

outside. The coils were wired in antiparallel, so that the field in the plane of symmetry of the two coils was zero, but the field gradient was non zero.
The coils were powered by a Quad™ audio frequency amplifier, fed from the internal reference of a lock-in amplifier. The coils were attached, and centred on the pole pieces with a 6.35 mm centred hole in the iron pole pieces. Proximity of the iron pole pieces has the effect of introducing a frequency dependence of the amplitude and phase of the gradient field. One way of overcoming this problem was to monitor the actual gradient field, with an additional set of coils, placed inside the coils used to generate the gradient [8, 14].

2.2.2 Resonant sample mount

The resonant system is the heart of the AGFM, which distinguishes it from conventional cantilever [18], or force magnetometry. It is advantageous to have high sensitivity, and mechanical gain (or Q factor). Design of the resonant element has received a great deal of attention in the literature, with many different solutions being proposed. All the previous designs have used a resonant cantilever, of some description, varying from 500 μm, to 200 mm long. An approximate mathematical treatment of the equations governing mechanical resonance led Zijlstra [3] to expressions for the mechanical quality factor (Q), and sensitivity (y_d/f_0) in terms of various physical quantities of the system. Given assumptions of light damping, and small displacements from equilibrium, these are;

$$Q \approx 0.3\left(\frac{d^3}{\eta l^2}\right)(\rho Y)^{1/2} \qquad (2.1) \qquad \left(\frac{y_d}{f_0}\right) \approx 2\left(\frac{l}{\eta d}\right)\left(\frac{\rho}{Y}\right)^{1/2} \qquad (2.2).$$

Here f_0 is the oscillatory force, y_d the dynamic displacement, η the dynamic viscosity of air, l the reed length, d the reed diameter, ρ the reed density, and Y is Young's modulus. Sidles *et al.,* [19] gave expressions for the eigenfrequencies and effective spring constant of a simple clamped cantilever with thickness t, and mass m;

$$\omega_0 = \begin{bmatrix} 3.516 \\ 22.03 \\ 61.70 \\ 120.9 \end{bmatrix} \frac{t}{l^2}\sqrt{\left(\frac{Y}{12\rho}\right)} \qquad (2.3) \qquad k_{mech} = \frac{m}{4}\omega_0^2 \qquad (2.4).$$

The important characteristics that the resonant system of an AGFM should possess are discussed below.

High sensitivity and Q factor

The Q factor is the factor by which the sensitivity at resonance (S_R) is increased by, over the static sensitivity (S_S);

$$S_R = S_S Q$$

These should therefore be large enough to enable detection of the moment of small or weakly magnetic samples. From equations 2.1 and 2.2, the conditions for optimum performance of the instrument are, in the case of high sensitivity; a long thin, dense and flexible reed. For maximal Q factor, the conditions are changed to; a short wide, dense and stiff reed. These requirements have to be balanced against the need for a short length scale, in order to achieve a sufficiently high resonant frequency. Q also determines the width of the resonance peak, with an excessively high Q value meaning an extremely narrow (and difficult to find) resonant peak. This would then require a very precise and minutely adjustable oscillator to stay on resonance, and allow for frequency drifts with temperature. The Q factor can be expressed as a measure of energy loss per vibration period, so for a high Q all loss mechanisms should be minimised. Previous work [5] indicates that air damping is the major loss mechanism at atmospheric pressure. A modest vacuum reduces this, as does a small surface area resonant element. Other possible loss mechanisms are internal mechanical hysteresis in the material, and losses through the support. Very low internal losses are predicted for a cantilever made of pure defect free materials, such as single crystal silicon [20], and silicon nitride (Si_3N_4). Energy losses from the resonant element through the support are reduced as the stiffness of the support increases. This can be achieved by making the resonant frequency of the support much lower (1-2 orders of magnitude) than the operating frequency [3].

Low magnetic moment

Since the sample mount is under the influence of the same fields as the sample, there will be an additional force acting upon it according to its magnetic moment, indistinguishable from those of interest. Obviously the lower the moment is, the

better, so that large background contributions are not present. The background should be repeatable, to the resolution required to extract the signal due to a sample, and ideally linear with field, and temperature. For this reason, ferromagnetic materials are unsuitable.

Suitable resonant frequency

Experience and common sense indicates that operation of any sensitive detectors anywhere near a multiple of 50 Hz, produces excessive amounts of interference from nearby, mains powered equipment. In addition, the energy spectrum of environmental noise is inversely proportional to frequency, so it is advantageous to have a high resonant frequency. A higher frequency also means that for a given *Q* factor, the system is quicker to respond to a change in driving force. There are several factors that affect the resonant frequency of a system, as shown in equation 2.3. There are also geometrical factors, due to the shape of the system, detailed given by Zijlstra [3]. There is the possibility of operating a resonant element at a higher harmonic frequency. From equations 2.3 and 2.4, the second flexural mode is expected at 6.3 times the fundamental frequency, and the effective spring constant increases by roughly a factor of 40. This implies an increase in Q factor, and a decrease in static sensitivity of a factor of 6.3, from examination of equations 2.1, and 2.2, which should give the same dynamic sensitivity.

Resilience

Any sample mount needs to accommodate macroscopic samples, and still yield accurate data. Sample mass has an effect on the resonance properties of the sample holder [7], increasing for large samples. Increasing the mass and thickness of the resonant sample mount reduces this effect, allowing larger samples to be measured. This would make the sample mounts less prone to breaking when changing sample. If it is intended to subject the sample to a range of temperatures, the properties of the sample holder must be suitable throughout the temperature range.

These individual requirements are not difficult to meet separately. However, when considered together, compromises had to be made to gain the best possible performance. The sample probes used were made from a number of quartz glass fibres, glued together with either cyanoacrylate or epoxy adhesive in a plane perpendicular to the axis of the magnets. The fibres were glued together at regular intervals, so that they vibrated together. Quartz was chosen, as the resonant properties are not affected by magnetic fields [21], and thin fibres were readily available at no cost, from a glassblowing workshop on site. The sample holder consisted of a piece of thin glass cut to size and glued to the end of the sample probe. The glass sample holder was also aligned in this plane for most of the probes. The samples were mounted onto the glass plates using a small amount of vacuum grease. For large thin samples, such as nickel foil, two pieces of glass, with the foil sandwiched between them. This was because thin samples had a tendency to twist so that the field was in the plane of the sample, rather than perpendicular to it. The probes were very fragile, and many were broken during the experiment, despite great care being taken when they were being removed or inserted into the apparatus. The quartz fibres used in the construction of the probes were noticeably tapered, with one end of a larger diameter than the other. An attempt was made to reduce the effect of this on the vibration by arranging fibres together in the completed probes so that the tapers of adjoining fibres ran in opposite directions. Due to this, and the fact that the average fibre diameters varied slightly, no two sample rods were identical, each having different resonant frequencies and Q factors. A photograph of the completed apparatus is shown in Figure 2.3, with a sample rod in place.

2.2.3 Vibration detection

A method of detecting the vibrations of the resonant sample mount was needed, robust enough to handle the mass of the sample and sample mount, and the stresses involved in changing the sample. Ideally it should be unaffected by both the applied field, field gradient, and changes in temperature.

Piezoelectric biomorph

The vibration-sensing element in the experimental system was a piezoelectric biomorph. This consisted of a thin ceramic plate, with a thin film of piezoelectric crystal deposited on both sides. The material used was lead-zirconium titanante (PZT), one of the most common piezoelectrics.

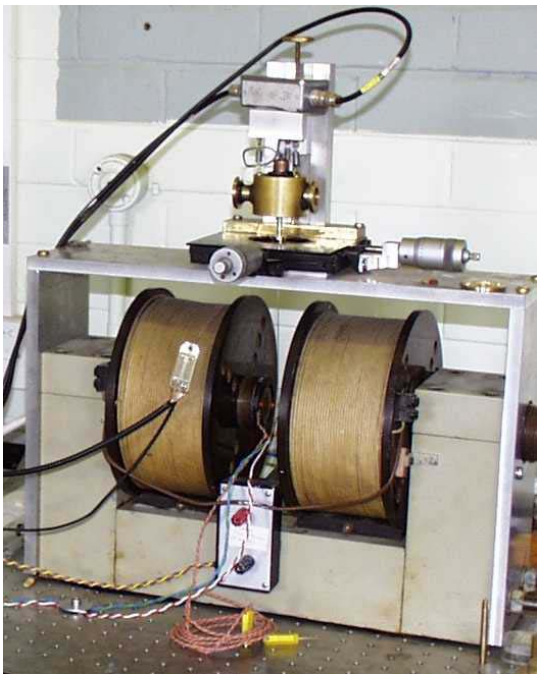

Figure 2.3. Photograph of the completed AGFM, set up for room temperature operation. The x-y-z stage can be seen above the magnet coils, with the brass damping block in place.

Piezoelectric materials produce electrical signals when they are deformed, and conversely deform when electrical signals are applied to them. They form the basis of quartz oscillators, and many types of electronic transducers. The devices used were supplied by RS Components Ltd, stock number 285-784, were 35 mm long, 1.5 mm wide, 0.6 mm thick, and had a response of 4 V peak-to-peak for a 0.01 mm vibration at the biomorph tip [22]. The actual deformation experienced in use was orders of magnitude smaller. Signals were typically of the order of 0.2 mV (corresponding to a calculated deformation of 5 Å at the biomorph tip). The sample probe was glued to the tip of a biomorph, with roughly 10 mm overlap. The position of the biomorph is shown in Figure 2.3.

Vibration isolation

It was impossible to find a location free from external sources of mechanical vibration, so isolating the instrument from these sources was necessary. The level of isolation should be such that levels of vibration at the measurement frequency are reduced as far as is possible. This will depend upon the measurement frequency used, and the bandwidth of the detection circuitry (e.g. dictated by the time constant on a lock in amplifier). Also present were vibrations at the measurement frequency from the gradient coils. The isolation was chosen to adequately screen noise of a broad bandwidth, from sub-Hertz building noise, to audio frequency ambient noise. It was therefore decided to have a number of layers of vibrational isolation. These took the form of a large brass block, suspended on three extension springs, as shown in Figure 2.3. This was designed to have a resonant frequency much lower than that used in the instrument. Additional isolation was provided by liberal use of rubber isolators, and placing the instrument on an optical bench. An attempt to reduce vibration by enclosing the sample and detector in an evacuated enclosure was unsuccessful, due to the extra vibrations introduced by the vacuum pump.

2.3 Vibrations of the AGFM probe

2.3.1 Resonant conditions

Due to the need to drive the AGFM probe to mechanical resonance, it was necessary to determine the exact resonance frequency, Q factor, and relative phase of the system before each measurement. The motion of the quartz fibre can be described using the equations of forced (or driven), damped harmonic motion, as given in equation 2.5. It was assumed that the deflections are small enough so that any restoring forces are linear with deflection.

$$z'' + 2\zeta z' + \Omega^2 z = a\sin(\omega t) \tag{2.5}$$

Where z is the deflection of the tip of the quartz fibre from its equilibrium position, and Ω is the resonant frequency of the undamped system (a measure of the restoring force towards equilibrium). ζ is a resistive term, due to losses in the fibre, and drag forces acting on the probe. The reduced driving force is $a\cdot\sin(\omega t)$, at a frequency $f = \omega / 2\pi$. The solution to this equation has two parts, a

steady state solution, and an exponentially decaying solution. It is the steady state solution that is of interest;

$$z = P' \sin(\omega t) + Q' \cos(\omega t).$$

Substituting this into equation 2.5, and solving for *P'* and *Q'* gives;

$$P' = \frac{-a(\Omega^2 - \omega^2)}{(\Omega^2 - \omega^2)^2 + 4\zeta^2\omega^2}, \qquad Q' = \frac{2a\zeta\omega}{(\Omega^2 - \omega^2)^2 + 4\zeta^2\omega^2}.$$

Combining these into a single oscillating term of general phase δ' gives;

$$z = \frac{a\sin(\omega t + \delta')}{\sqrt{(\Omega^2 - \omega^2)^2 + 4\zeta^2\omega^2}}, \qquad \delta' = \tan^{-1}\left(\frac{Q'}{P'}\right). \tag{2.6}$$

To find the resonant frequency, one needs simply to find the value of ω that gives a maximum in *z*. This is calculated by;

$$\omega_C^2 = \Omega^2 - 2\zeta^2.$$

If the AGFM is well designed, the damping term, ζ will be much smaller than Ω, the restoring term. Therefore, the resonant frequency would be only slightly lower than the case without any damping at all. The maximum amplitude of vibration is found by substituting the resonant frequency, ω_c into the general term for *z* (equation 2.6), giving;

$$z_{\max} = \frac{a}{2\zeta\sqrt{\Omega^2 - \zeta^2}}. \tag{2.7}$$

The phase of the oscillation with respect to the driving force is given by;

$$\delta_c' = \tan^{-1}\left(\frac{-\omega_c}{\zeta}\right).$$

This tends to –90 °, as the damping is reduced towards zero (i.e. as *P'* approaches zero). The *Q* factor can be found by comparing the maximum value of the displacement at resonance (equation 2.7) with the static displacement away from resonance. The static displacement (response to a constant force, or an oscillating force well removed from resonance) can be obtained either by disregarding all differentials of *z* in equation 2.5, or by constraining ω to zero in equation 2.6. This gives in the limit of small damping (large *Q* factor);

$$z_s = \frac{a}{\Omega^2}, \qquad Q = \frac{\Omega^2}{2\zeta\sqrt{\Omega^2 - \zeta^2}} \approx \frac{\Omega}{2\zeta}.$$

This allows an expression for *P'* and *Q'* in terms of resonant frequency, and *Q* factor.

$$P' = \frac{-a\left(\omega_c{}^2 - \omega^2\right)}{\left(\omega_c{}^2 - \omega^2\right)^2 + \dfrac{\omega_c{}^2\omega^2}{Q^2}} \quad (2.8), \qquad Q' = \frac{a\dfrac{\omega_c\omega}{Q}}{\left(\omega_c{}^2 - \omega^2\right)^2 + \dfrac{\omega_c{}^2\omega^2}{Q^2}}. \quad (2.9)$$

As can be seen from equations 2.8, and 2.9, the component in phase with the driving force, *P'* disappears when at the resonant frequency. This gives a potentially useful indicator as to when the system is on resonance. However, since these expressions are approximations, this is not the case in reality (the expression for the phase when on resonance is ≠ 90 °). To find the frequency at which *P'* is zero, for the case where damping is taken into account fully is a little more complex. The exact expression for *P'* is found to be;

$$P' = \frac{-a\left(\dfrac{\omega_c{}^2 Q}{\sqrt{Q^2-1}} - \omega^2\right)}{\left(\omega_c{}^2 - \omega^2\right)^2 + \dfrac{\omega_c{}^2\omega^2}{\left(Q^2-1\right)}}. \quad (2.10)$$

As can be seen, this is non zero when on resonance, with a value of;

$$P' = -\frac{a}{\omega_c^2}\left(1 + Q\sqrt{Q^2-1} - Q^2\right). \quad (2.11)$$

This can be simplified by replacing the term inside the brackets of equation 2.11 with its Maclaurin series [23] in powers of $1/Q$. Neglecting terms of order $1/Q^4$ and higher yields an approximation of;

$$P' \approx -\frac{a}{2\omega_c^2}\left(1 - \frac{1}{Q^2}\right) \approx -\frac{a}{2\omega_c^2}$$

For an expected operating frequency of the order of 100 Hz, this is negligible compared to the peak amplitude. Also using the exact expression for *P'* (equation 2.10), the point at which it is exactly zero is when;

$$\omega = \frac{\omega_c}{\sqrt[4]{1 - \dfrac{1}{Q^2}}} \approx \omega_c\left(1 + \frac{1}{4Q^2}\right).$$

Using a frequency of 100 Hz, and a *Q* factor of 200, the calculated deviation of the zero crossing point from resonance is 0.625 mHz, which is below the

resolution of the frequency source in the lock-in amplifier. At much lower Q factors and frequencies, these factors may become important, but the approximation of zero crossing of P' at resonance has been taken to be valid in normal operation. This treatment can be extended, to cover the higher order resonances.

Flanders [7] gives solutions for a general resonance order;

$$X = af_0 f \frac{\left(\frac{f_n f}{Q}\right)}{\left(\frac{f_n f}{Q}\right)^2 + (f_n^2 - f^2)^2} \quad (2.12), \quad Y = af_0 f \frac{(f_n^2 - f^2)}{\left(\frac{f_n f}{Q}\right)^2 + (f_n^2 - f^2)^2}$$

(2.13)

Where X and Y are the in phase and quadrature signals respectively. These correspond to equations 2.8, and 2.9 from the treatment above. f_0 is the centre frequency of the first (fundamental) resonance peak, and f_n is the centre frequency of the resonant peak in question. These equations assume that the resonant element is of uniform density and stiffness along its length, the deflection along the element can be approximated as the sum of travelling waves, and the support is immovable. None of these assumptions are valid for an AGFM, as the sample mass is localised at one point on the resonant element. The travelling wave model assumes that the free end of the rod has an angular deflection of zero, whereas the angular deflection is maximised at the free end. In addition, Flanders used a biomorph detector, between the resonant element, and the support; thus, the support presented to the resonant element was not infinitely stiff.

2.3.2 Resonant peak fitting

A signal is said to be in phase, if the X component is maximised at the resonant frequency. Knowledge of the above equations, and data for the X, and Y signals in the region of the resonant frequency allows an optimisation routine to be used. This fits a number of parameters to a dataset, such as resonant frequency, Q factor, peak height, etc. Unfortunately, there is a phase change inherent in the response of the system due to the audio amplifier and pole piece effects, so not

only does the centre frequency need to be found, but this phase lag needs to be found also. In general, the lock-in signal outputs will be as follows,

$$X^* = X\cos(\theta) + Y\sin(\theta), \qquad Y^* = X\cos(\theta + \pi/2) + Y\sin(\theta + \pi/2).$$

To find the correct phase and frequency for measurements, both the in-phase, and out of phase components are measured, over a narrow frequency range centred on the frequency of interest, an example of which is given in Figure 2.4.

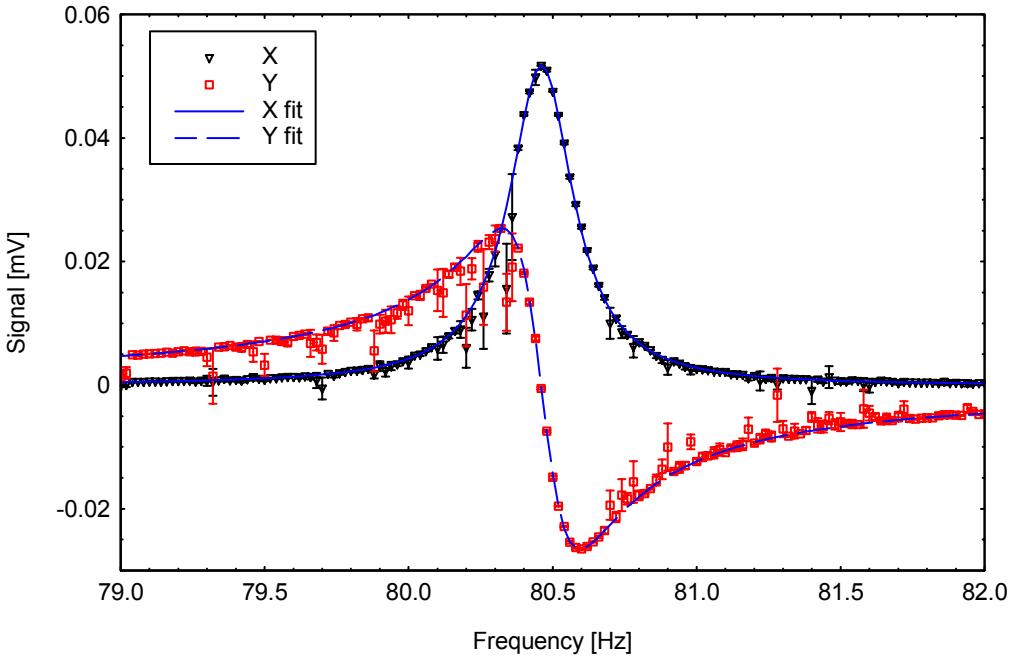

Figure 2.4. Illustration of the uneven errors encountered when looking at small signals. Lines are fits to the data points.

These curves are modelled simultaneously, in a spreadsheet application. This also gives information about any instrument offsets present, and the quality factor of the resonance. The application accepts data in 5 columns, corresponding to frequency, X^* signal, X^* noise, Y^* signal, Y^* noise. The noise values are the standard deviation of a number of measurements taken under identical conditions, separated in time by a delay of at least 5 times the time constant of the lock – in amplifier. The variable parameters are; phase, resonant frequency, vibration amplitude, Q factor, and offsets in the X^*, and Y^* signals. A trial fit dataset is constructed from the initial values of the variable parameters, and a difference table calculated. From the difference table, a fitting parameter, F is obtained;

$$F = \sum_f \frac{|X^*(f) - X_{FIT}^*(f)|}{\sigma_X + \sigma_A} + \sum_f \frac{|Y^*(f) - Y_{FIT}^*(f)|}{\sigma_Y + \sigma_A} \quad (2.14)$$

Where $X^*(f)$, $X^*_{FIT}(f)$, and σ_X are the data point, trial fit, and data noise respectively. A weighting of $1/(\sigma_X + \sigma_A)$ was applied in order to minimise the influence of rogue data points from noisy datasets. These points were found away from the main curve, and were caused by some transient vibration source (such as a door slamming). The addition of σ_A is necessary for the case where the noise present is below the resolution of the lock-in amplifier, and a value of zero for σ_X would result in an infinite term in the series. σ_A is the average noise value for the entire dataset.

A new set of the variable parameters are chosen, that reduce the value of the fit parameter F. The process is repeated until no further improvement is possible, within a set tolerance. The fitting procedure is automated within the spreadsheet, including choosing of sets of variable parameters. It was found that the initial guesses needed to be reasonably accurate for the automatic fitting procedure to commence. The fitting procedure was found to be robust, allowing 'difficult' datasets to be analysed, such as in Figure 2.4, where the noisy data points were displaced to lower amplitude values. The cause of this particular type of error is unknown. This has been successfully analysed, due to the greater weighting of points with smaller noise values. The same is true for the data in Figure 2.5, where the increased electrical noise due to interference from mains powered equipment is clearly visible around 100 Hz. The resonant peak height is approximately an order of magnitude lower than the one shown in Figure 2.4.

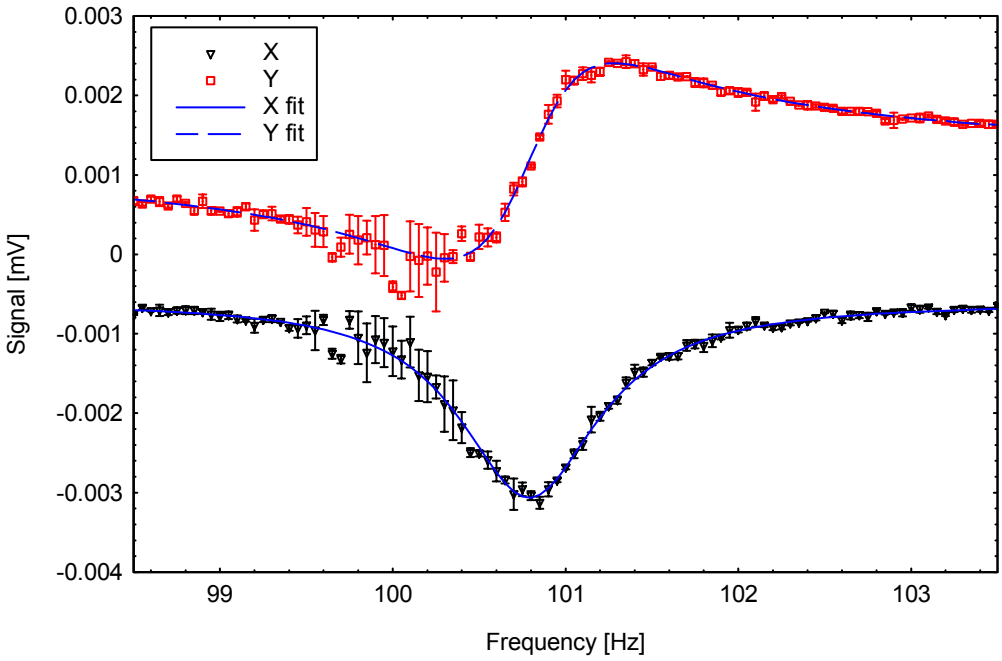

Figure 2.5. The effect of noise at 100 Hz. The lines are fits to the resonant function. The offsets are large compared with the signal.

The signal offsets are now clearly visible. These are caused by biasing errors in amplifier stages, and crosstalk from leads supplying the gradient coils, to the biomorph connections. Once the correct frequency and phase are known, it is possible to obtain the maximum output signal, working on the peak of the in-phase component (i.e. at f_n). The peak value of X is;

$$X_{MAX} = \frac{af_0Q}{f_n} \quad . \tag{2.15}$$

Usually, there is no reason not to operate at the fundamental frequency, f_0. However, it was soon found that once determined, the resonance frequency was not stable from hour to hour, and day to day. This was noticed because of the sensitivity of the out of phase signal to small changes in resonant frequency, due to it having maximum gradient at resonance, where it crosses through zero. The reasons for this are discussed in section 3.2. There are two possible approaches to eliminating the errors produced when the resonant frequency changes. One can attempt to continuously alter the frequency of the signal applied to the gradient coils, and stay on resonance, or the measurement frequency can remain fixed, and corrections be made to the data according to the calculated resonant frequency. Initial attempts to continuously update the measurement frequency during data collection proved difficult, especially as the field was varied through

zero. The increased number of measurements necessary to determine resonance conditions slowed data collection to a considerable degree. It was decided to operate at fixed frequency for all but a few experiments thereafter.

2.3.3 Off-resonance corrections

This procedure enables the variation in resonant frequency to be tracked as an experiment is being run, or later when the data is being analysed. Starting from any point on the resonance curve, one can, with knowledge of both *X*, and *Y* components of the data, find the height, and centre frequency of the resonance. These calculations are assuming *Q* factor, and phase stay unchanged throughout the experimental run. From inspection of the equations given by Flanders, (equations 2.12 and 2.13), and the expression for the maximum height of the resonance peak (equation 2.15), it can be seen that this is given by;

$$X_{MAX} = X(f_0) = X(f) + \frac{(Y(f))^2}{X(f)}. \qquad (2.16)$$

By dividing equation 2.13 by equation 2.11, and re-arranging, the centre frequency can be expressed as;

$$f_0 = \frac{f}{2}\left(\sqrt{4 + \left(\frac{Y(f)}{QX(f)}\right)^2} + \left(\frac{Y(f)}{QX(f)}\right)\right)$$

The only variables needed in these equations are the values of *X*, and *Y*, and the *Q* factor. In practice, knowledge of the experimental offsets is also required. Examples of data that have been treated in this way are shown in section 3.4. The assumptions that the phase and *Q* factor remain approximately stable are borne out by experiment (see section 3.3). In order to obtain any meaningful results from this technique, the measurement frequency needs to be within the main part of the resonant peak. If this is not the case, the errors become very large as is illustrated in Figure 2.6. This was obtained from resonance curve data, similar to that in Figure 2.4. The resonance curve was first fitted, using the procedure outlined above, to get accurate values for the *Q* factor, and the peak amplitude.

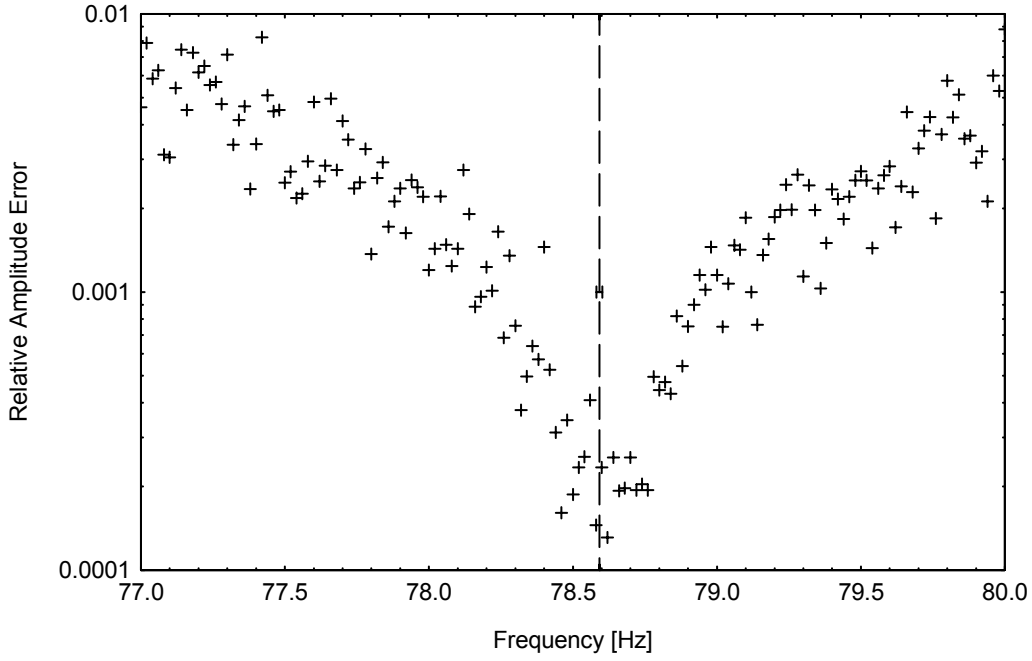

Figure 2.6. Standard error on the reconstructed peak amplitude. The resonant frequency, as determined from a fit to the resonant curve is marked (78.952(10) Hz). The error on the plotted points lies within the data markers.

Then taking the individual X and Y values collected at each measurement frequency, and the Q value already obtained, a calculation of the reconstructed peak height was made using equation 2.16. The error on this quantity was also calculated, due to the uncertainty in the precise values of X, Y, Q, and the calibration constant for the probe, C. Uncertainties in the values of X, and Y were obtained from the standard deviation of the collected data points. The uncertainty in Q was estimated from the variation of fitted values to a number of resonant curves measured with the same sample mounted. The sample used for these measurements was 31.7(8) mg of quartz glass. The largest contribution to the uncertainty in the calibration constant, C was due to the uncertainty on the measurement of the sample mass. The formula for the standard error on the reconstructed peak amplitude is;

$$\frac{\sigma_{X_{MAX}}}{X_{MAX}} = \frac{\sqrt{\left[\left(\left|\sigma_X\left(1-\left(\frac{Y}{X}\right)^2\right)\right| + \left|2\sigma_Y\frac{Y}{X}\right|\right)C\right]^2 + \left[\frac{X_{MAX}\sigma_C}{C}\right]^2}}{X_{MAX}}.$$

Similarly, the standard error on the reconstructed resonant frequency is;

$$\frac{\sigma_{f_n}}{f_n} = \frac{\left|\left(\frac{fY}{2XQ}\right)\left(1+1\Big/\sqrt{1+\left(\frac{2QX}{Y}\right)^2}\right)\left(\left|\frac{\sigma_X}{X}\right|+\left|\frac{\sigma_Y}{Y}\right|+\left|\frac{\sigma_Q}{Q}\right|\right)\right|}{f_n}.$$

The uncertainty in f, the measurement frequency is quoted as 10^{-3} Hz in the manual for the lock-in amplifier. This is insignificant compared to the other sources of error, and so has been ignored. As can be clearly seen from Figure 2.6, the uncertainties associated with the fitting technique increase rapidly as the measurement frequency diverges from the resonant frequency. The data presented here was taken under optimal conditions, in a steady applied magnetic field. The sample mass was small, so environmental noise was reduced. The ambient temperature was stable during data collection, the DC field coils having been left powered for a number of hours before the measurement took place.

2.4 Summary

The available literature concerning the development and evaluation of various AGFMs shows many varied attempts, the first being Zijlstra [3]. Many more followed, refining and adapting that which had gone before. Amongst these, of note is the design of Richter *et al.,* [8], who achieved an optimum magnetic moment resolution of 10^{-14} JT^{-1}, although only when measuring micron sized particles. Richter *et al.,* and most before, used piezoelectric detection elements, but Gibson *et al.,* [11] used optical interferometry to achieve a comparable resolution, albeit with a similar limit upon sample sizes. All of those instruments that allowed the study of macroscopic samples (Reeves [4], Frey *et al.,* [9], and the commercially available system evaluated by O'Grady *et al.,* [12]) obtained somewhat lower resolutions. A number of authors successfully demonstrated variable temperature operation, unfortunately with an accompanying loss of resolution. The limiting factor in terms of resolution of nearly all instruments reported seems to be the effects of ambient vibration on the detection elements. In view of the previous work done, and the expertise available to the author, it was decided to use piezoelectric detection for the present instrument. These also had the advantage of being readily available, and easily interfaced to a lockin amplifier. The resonant element was chosen to be quartz, as this was readily available, and had been successfully used in many of the previous instruments, in

various sizes of drawn fibre. Attention was paid to the dimensions of the resonant fibre, in order to obtain a suitable stiffness, resonant frequency, and *Q* factor. In order to eliminate as much as possible the environmental vibrations that have been the limiting factor in improving resolution of other instruments, attention was paid to the vibration isolation employed. Several methods were used to screen the detection mechanism from both acoustic (airborne), and structural ambient vibrations.

The DC magnetic field, and alternating field gradient were realised in a conventional manner, using an electromagnet, and opposition wound air cored coils respectively. Both of these elements were placed under automated computer control, as was the lockin amplifier used to measure the output of the piezoelectric element. A block diagram of the control equipment is given in Figure 2.2.

A thorough mathematical treatment of the mechanical vibration is presented in section 2.3 above. Due to the mechanical resonant frequency not being sufficiently stable during a sequence of measurements, it was found necessary to correct the measured signals for frequency error. This entailed measuring the resonant curves to establish the correct phase and *Q* factor, and applying a correction term to the measured signals. The correction term needed has been determined from the relevant equations of motion, and a treatment of the ensuing uncertainties of measurement has been given. As expected, the lowest measurement uncertainties are obtainable when the measurement frequency is the same as the mechanical resonant frequency. The application of correction factors, and associated measurement uncertainties has been routinely applied to all the measured data from the AGFM, by means of a standard measurement procedure, and analysis spreadsheets.

References

1. Flanders, P. J. and Graham Jr, C. D., *Rep. Prog. Phys.* **56** (1993) 431.
2. Chikazumi, S., *Physics of Ferromagnetism.* 2nd Edition. The International Series of Monographs on Physics, ed. Birman, J., *et al.,*. Published by; Clarendon Press, Oxford (1997)
3. Zijlstra, H., *Rev. Sci. Instrum.* **41** (1970) 1241.
4. Reeves, R., *J. Phys. E* **5** (1972) 547.
5. Roos, W., *et al.*, *Rev. Sci. Instrum.* **51** (1980) 612.
6. Schippan, R. and Hempel, K. A., *J. Appl. Phys.* **53** (1982) 7867.

7. Flanders, P. J., *J. Appl. Phys.* **63** (1988) 3940.
8. Richter, H. J., Hempel, K. A. and Pfeiffer, J., *Rev. Sci. Instrum.* **59** (1988) 1388.
9. Frey, T., Jantz, W. and Stibal, R., *J. Appl. Phys.* **64** (1988) 6002.
10. Flanders, P. J., *Rev. Sci. Instrum.* **61** (1990) 839.
11. Gibson, G. A. and Schultz, S., *J. Appl. Phys.* **69** (1991) 5880.
12. O'Grady, K., Lewis, V. G. and Dickson, D. P. E., *J. Appl. Phys* **73** (1993) 5608.
13. Wallace, J. L. and Espinoza-Faller, F. J., *Meas. Sci. Tech.* **6** (1995) 1221.
14. Zimmermann, G., *et al.*, *IEEE Trans. Mag.* **32** (1996) 416.
15. Asti, G. and Solzi, M., *IEEE Trans. Mag.* **32:**(5), (1996) 4893.
16. Asti, G. and Solzi, M., *Rev. Sci. Instrum.* **67:**(10), (1996) 3543.
17. Hill, E. W., Nazran, P. and Tailor, P., *IEEE Trans. Mag.* **32** (1996) 4899.
18. Dam, N.-E., Guldbrandsen, T. and Jacobsen, C. S., *Meas. Sci. Tech.* **4** (1993) 42.
19. Sidles, J. A., *et al.*, *Rev. Mod. Phys.* **67** (1995) 249.
20. Witek, A. and Onn, D. G., *J. Vac. Sci. Tech.* **B9** (1991) 639.
21. Spassov, L., *et al.*, *Sensors and Actuators A* **62** (1997) 484.
22. RS Components, http://www.rs.co.uk/home (Accessed on; 12 July 2001)
23. Jeffrey, A., *Mathematics for Scientists and Engineers.* 4 Edition Published by; Chapman and Hall, London (1989)